Physics of the Earth and Planetary Interiors, 33 (1983) 284–303
Elsevier Science Publishers B.V., Amsterdam – Printed in The Netherlands

The Gilbert Islands (Republic of Kiribati) earthquake swarm of 1981–1983

Thorne Lay

Seismological Laboratory, California Institute of Technology, Pasadena, CA (U.S.A.)

Emile Okal *

Department of Geology and Geophysics, Yale University, New Haven, CT (U.S.A.)

(Received July 28, 1983; accepted August 24, 1983)

Lay, T. and Okal, E., 1983. The Gilbert Islands (Republic of Kiribati) earthquake swarm of 1981–1983. Phys. Earth Planet. Inter., 33: 284–303.

A major swarm of intraplate earthquakes at the southeastern end of the Gilbert Islands Chain (3.5°S, 177.5°E) commenced in December 1981 and lasted through March 1983. No seismicity had been reported in the historical record in this region prior to 1981, but during the swarm 217 events with $m_b \geq 4.0$ were located by the NEIS, with 86 events having $m_b \geq 5.0$. The source region is quite remote, and the uniform detection level for the NEIS is for $m_b \geq 4.8$. A b-value of 1.35 is found for the swarm using the maximum likelihood method. Four events in the sequence were large enough ($m_b = 5.6–5.9$) to determine focal mechanisms teleseismically using body- and surface-wave analysis. These events are found to have a range of mechanisms, from predominantly thrust with a significant oblique component, to purely strike-slip. The compression axes are consistent for all four events, with horizontal orientation trending NNE–SSW. This orientation is perpendicular to the direction of plate motion. The events are located at depths between 15 and 20 km placing them deep in the oceanic crust or in the upper mantle. No obvious bathymetric feature can be related to the fault plane orientations, though there is an offset in the island chain near the epicenters. While some characteristics of the swarm suggest a magmatic origin, the nature of the focal mechanisms, the location of the swarm, and the large accumulated moment release of the sequence favor a tectonic origin.

1. Introduction

The Gilbert Islands, part of the recently constituted Republic of Kiribati, lie near the equator in the Central Pacific Ocean. These islands are well-removed from any major tectonic boundaries and lie on oceanic floor of Cretaceous age, in the center of a northwest trending island chain comprised of the Marshall, Gilbert and Ellice Islands (Fig. 1a). In December 1981, an earthquake swarm commenced at a location ~ 150 km southeast of Arorae Island, which is the southeasternmost of the Gilbert Islands. Prior to this swarm there had been no previous seismic activity in this region reported in the historical record, and there is no record of recent volcanism. The swarm persisted until March 1983. Figure 1 indicates the epicenters of the earthquakes in 1981–1983, as determined by the NEIS. The locations define a diffuse cluster of activity spread over a 50 km long region. The nearest seismograph is ~ 14.3° to the south, and the station coverage to the north is almost non-ex-

* Present address: Department of Geological Sciences, Northwestern University, Evanston, IL, U.S.A.

0031-9201/83/$03.00

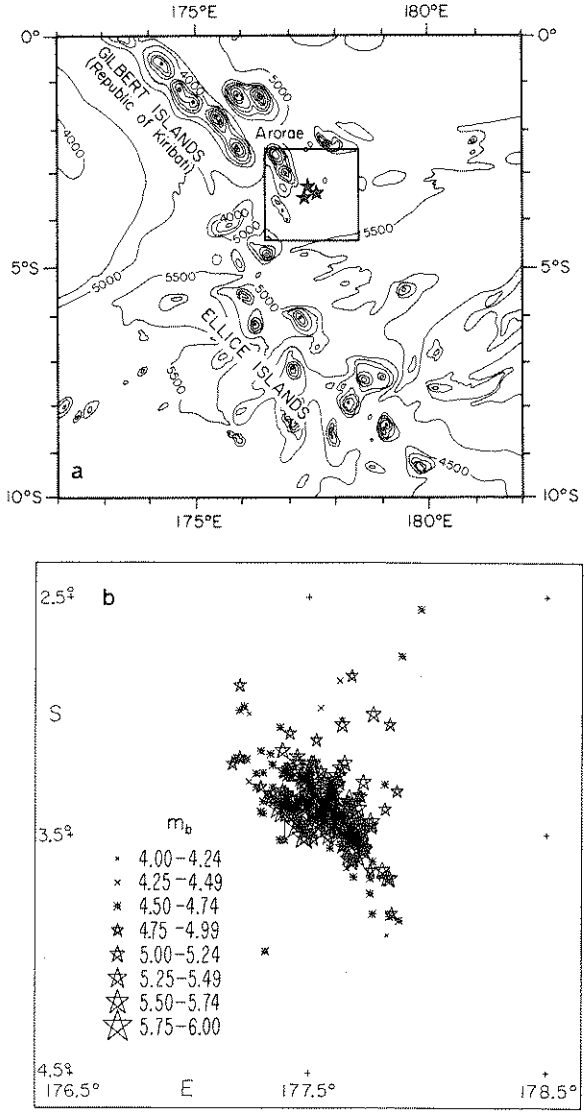

Fig. 1. (a) Base map showing the location of the largest events in the Gilbert Islands swarm and the Gilbert and Ellice Island chain (bathymetry contours are in m). The seismicity detected by the NEIS in the box is shown in (b).

istent, so there is relatively large uncertainty in the locations, and depth control is minimal.

There are few bathymetry determinations near the epicentral region, but the ocean floor appears to be fairly smooth at a depth of 5000 m in the available data (Mammerickx et al., 1974). Note that this region is the site of a major jog in the island chain, with the Ellice Islands being offset ~ 200 km to the southwest. There is no major transverse feature in the published bathymetry associated with this offset and no data is available regarding any age progression along the island chain. Even considering the largest magnitude events alone, there is no clear lineation apparent in the epicentral distribution. This paper reports detailed body- and surface-wave modeling of the four largest events of the swarm and discussion of the significance of this remarkable sequence.

2. Data analysis

The temporal behavior of the Gilbert Islands earthquake swarm shown in Fig. 1 is illustrated in Fig. 2. The magnitudes are m_b as reported by the NEIS. The data were taken from the Monthly Listings of the NEIS for the period through January 1983, after which the data source was the Preliminary Determination of Epicenters. The latter source is incomplete for events with magnitudes < 5.0, and the given epicenters and magnitudes are subject to revision. Note that the swarm activity appears to diminish in the latter half of 1982, but then resurges slightly in early 1983 before terminating in March.

Figure 2 shows that the largest events in the swarm have magnitudes of $m_b = 5.6$–5.9. Due to the restricted station distribution and the variability of the focal mechanisms as determined below, these magnitudes must be considered only rough estimates of the relative event sizes. The largest moment events occurred in the first 5 months of 1982. In a preliminary compilation of macroseismic data, Groves (1983) reports that events on January 7, 20 and 27, and February 15 were felt on Arorae Island, but that there are no reliable reports of tsunami damage, or uplift on the island.

Figure 3 shows the magnitude–frequency relation found for the swarm using the NEIS data. Both the cumulative number of events greater than or equal to each magnitude, and the number of observations with each magnitude are shown. It appears that the detection capability is relatively complete for events with $m_b \geq 4.8$. This high threshold is due to the remoteness of the source

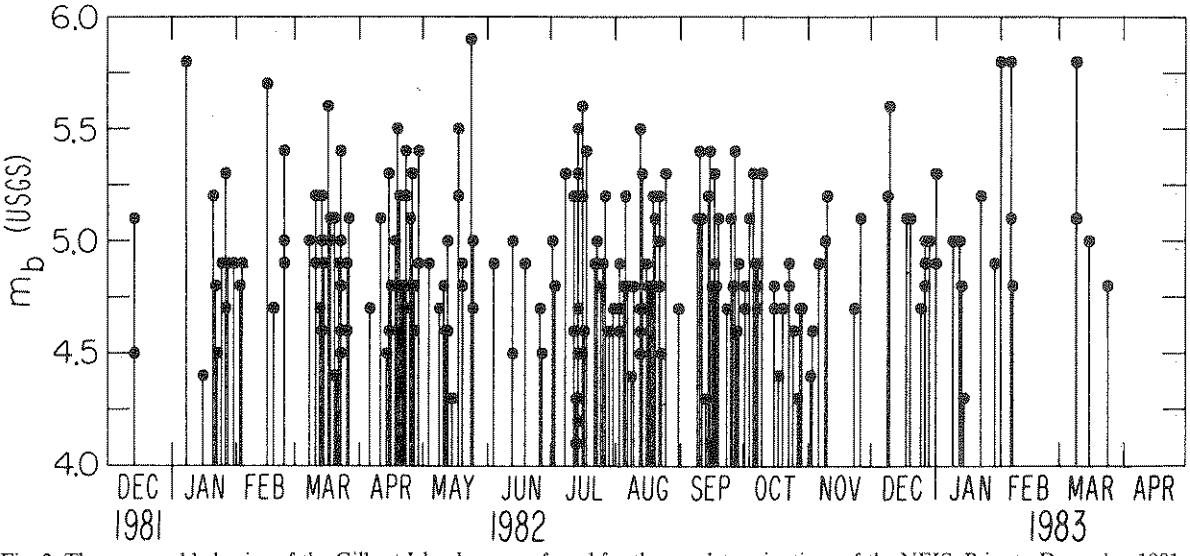

Fig. 2. The temporal behavior of the Gilbert Islands swarm found for the m_b determinations of the NEIS. Prior to December 1981 no seismicity had been detected in the region in the historic record. The data for February and March are from the Preliminary Determination of Epicenters, and all other data are from the NEIS Monthly Listing.

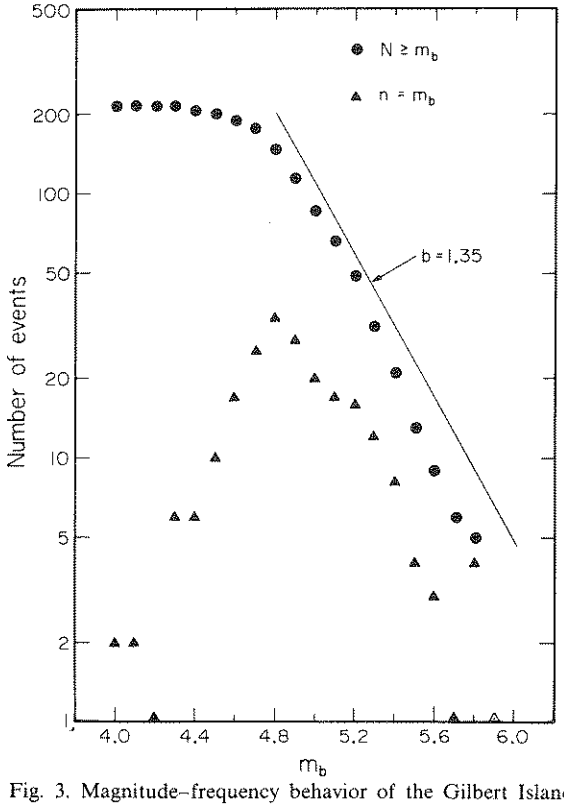

Fig. 3. Magnitude–frequency behavior of the Gilbert Islands swarm. The circles (●) indicate the cumulative number (N) of events greater than or equal to each m_b value, and the triangles (▲) indicate the number (n) of observations with each magnitude. The line shows the slope for a b-value of 1.35.

region. Following Utsu (1966) and Aki (1965), the b-value in the magnitude–frequency relation determined by the maximum likelihood method is b = 1.35, for $m_b \geq 4.8$. This slope is indicated by the line in Fig. 3. The narrow magnitude range available produces substantial uncertainty in the b-value estimate. The b-value of 1.35 is somewhat higher than the global average, estimated to be 0.9 by Gutenberg and Richter (1954) and 0.78 by Sakuma and Nagata (1957). Sykes (1970) determined a b-value of 1.3 for swarms in the northern Mid-Atlantic Ridge, whereas Francis (1968) determined b = 1.73 for 79 median rift events along the same ridge. The 1968 Fernandina caldera collapse in the Galapagos Islands had a complex frequency–magnitude behavior, with b = 1.24 for magnitudes below $m_b = 4.9$, and b = 2.53 for larger events (Francis, 1974). Volcanic activity is associated with a wide range of b-values, typically larger than 2, though lower values are found, such as b = 1.05 for long term activity in Hawaii (Furumoto et al., 1973); b = 1.3–3.2 for volcanic swarms in Tahiti–Mehetia (Talandier and Kuster, 1976), and b = 1.4 for microearthquakes at Mount Katmai, Alaska (Matumoto and Ward, 1967). Clearly, the b-value alone cannot characterize the Gilbert Islands swarm and only by analysis of the

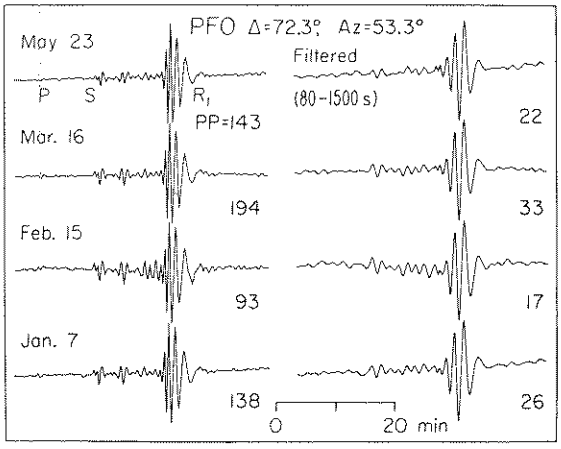

Fig. 4. Comparison of long-period recordings of four of the swarm events made at the IDA station PFO. The peak-to-peak (PP) amplitude in digital counts is shown for each trace. The traces on the right have been band-pass filtered to emphasize the long periods. The February 15 events shows relatively larger amplitude arrivals between the S- and Rayleigh-wave arrivals, indicating that it has a different mechanism from the other events.

seismic signals generated by the events can more be learned about the nature of the swarm.

Figure 4 shows a comparison of the long-period vertical recordings of four of the Gilbert Islands swarm events at the IDA station PFO. These four events are studied in detail below and their source parameters are given in Table I. In Fig. 4 it is quite apparent that these events are part of an earthquake swarm in that no event stands out as a mainshock. It is also apparent that the event of February 15 has a mechanism slightly different from the others, given the enhanced overtone excitation for that event.

Using the now standard procedures for modeling long-period P and SH waves (Langston and Helmberger, 1975; Kanamori and Stewart, 1976), the focal mechanisms of the four large events were determined. For this analysis we combined data from the WWSSN and GDSN networks because of the limited number of useable records recorded for these moderate size, remotely located events. Since no independently known source region crustal structure was available, we initially modeled the events as being in a half-space. The take-off angles were taken from the JB model calculations of Ritsema (1958) for a source region P velocity of 7.75 km s^{-1} and S velocity of 4.35 km s^{-1}. The average velocities above the source were 6.4 km s^{-1} for P waves and 3.7 km s^{-1} for S waves. While such half-space models are clearly oversimplified, the source orientations can be well-determined, along with minimum source depths. Using more realistic source structures allows additional features in the waveforms to be modeled thus improving the depth resolution, but this does not place much further constraint on the orientations.

Figure 5 shows the results of forward modeling of the P and SH waves for the event of January 7, 1982. This is the least well-constrained mechanism of the four presented here. The source depth used in the modeling was 11 km, and a 3 s duration trapezoid (1.0 s rise, 1.0 s constant, 1.0 s fall) was used. Note the difference in period of the WWSSN and digital network data. The latter is devoid of fine-scale features and is not even particularly sensitive to first motion in the vicinity of nodal orientations. In determining the model in Fig. 5 and for subsequent events, the waveform features that were found to be most diagnostic of the mechanism were the following. For such shallow events, the ratio of the second upswing to first upswing in the WWSSN P waveforms is indicative of the oblique component, as this ratio increases with increasing oblique motion. The large oscilla-

TABLE I

Event (1982)	Origin time	Lat. (°S)	Long. (°E)	m_b	M_S
January 7	08:42:52.7	3.39	177.57	5.8	5.4
February 15	05:50:12.2	3.51	177.48	5.7	5.6
March 16	00:20:43.9	3.32	177.53	5.6	5.6
May 23	21:32:35.1	3.39	177.40	5.9	5.7

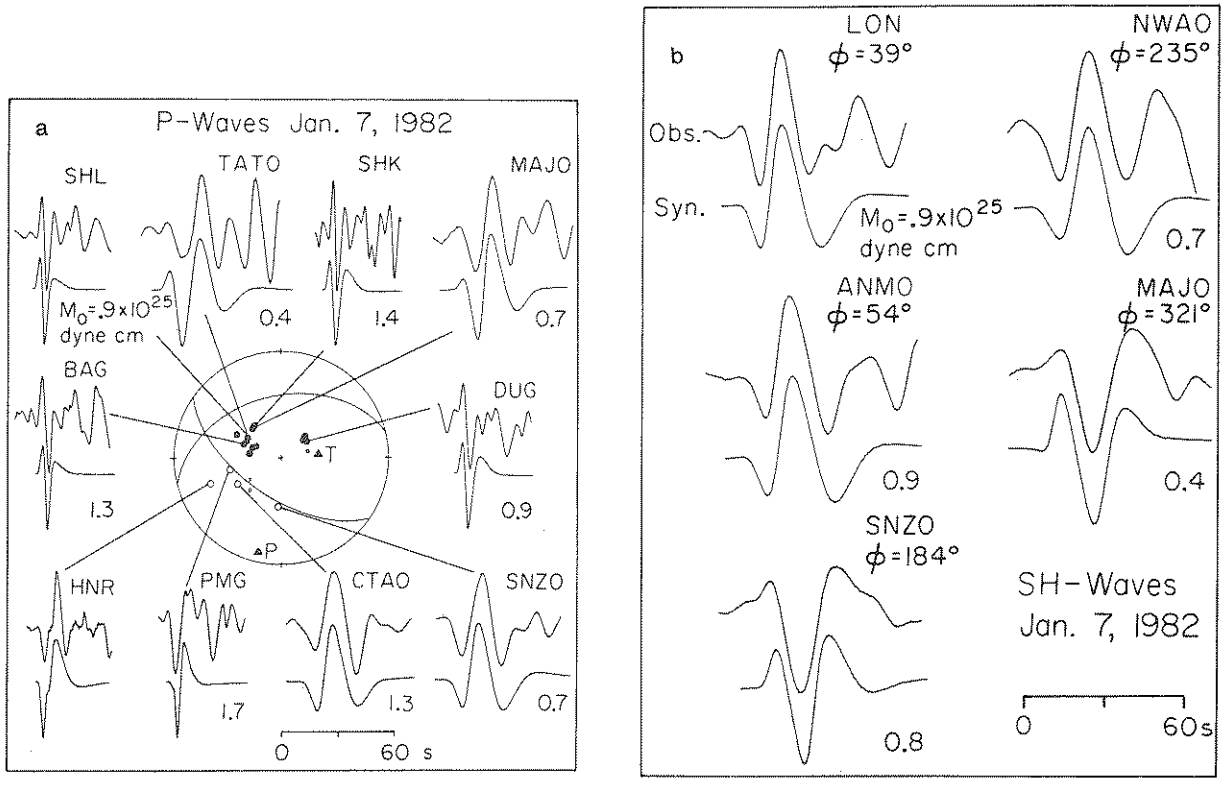

Fig. 5. P wave (a) and SH wave (b) observations and half-space synthetic seismograms for the event of January 7, 1982. The P-wave focal mechanism is shown in a lower hemisphere equal area projection, with solid symbols indicating compressional first arrivals. The moment from each station comparison is given, except for HNR which is at upper mantle distance. Note the long-period nature of the GDSN data (stations TATO, MAJO, CTAO, SNZO) compared with the WWSSN data. The half-space models have a source depth of 11 km, and all other parameters are as given in Table II.

tions ~ 20 s after the P arrival are produced by $_{pw}$P arrivals, as shown below. Thus, the second downswing at the digital stations like CTAO is often affected by water multiples and is not diagnostic of the source orientation. We also relied on the SH-wave polarizations and waveforms as observed at the digital stations in order to constrain the orientation of the northward dipping plane. The slight upward first motion at MAJO is most sensitive to this parameter. For the event of January 7 the P waves yield an average moment of 1.1×10^{25} dyne cm and the SH waves give 0.8×10^{25} dyne cm. The overall body-wave average moment is 1.0×10^{25} dyne cm. The mechanism is predominantly thrust with a nearly horizontal compression axis, but there is a resolvable oblique component. The strike is $\phi = 125°$, dip $\delta = 60°$ and rake $\lambda = 120°$. There is about a 10° uncertainty in each parameter given the assumptions made in the modeling and the mediocre data quality. If the fault geometry is circular, and the effective stress is equal to the stress drop, then the radius of the circular fault, a, is proportional to the total source time duration, T, and is given by (Ebel et al., 1978)

$$a = (28\pi\beta T)/[64 + 7\pi(5 + 4\sin\sigma)] \qquad (1)$$

where β is the shear velocity, and σ is the angle between the normal to the fault plane and the ray direction. Using this expression, the fault areas estimated for the two fault planes are 64 and 69 km^2. The corresponding stress drops are 47 and 42

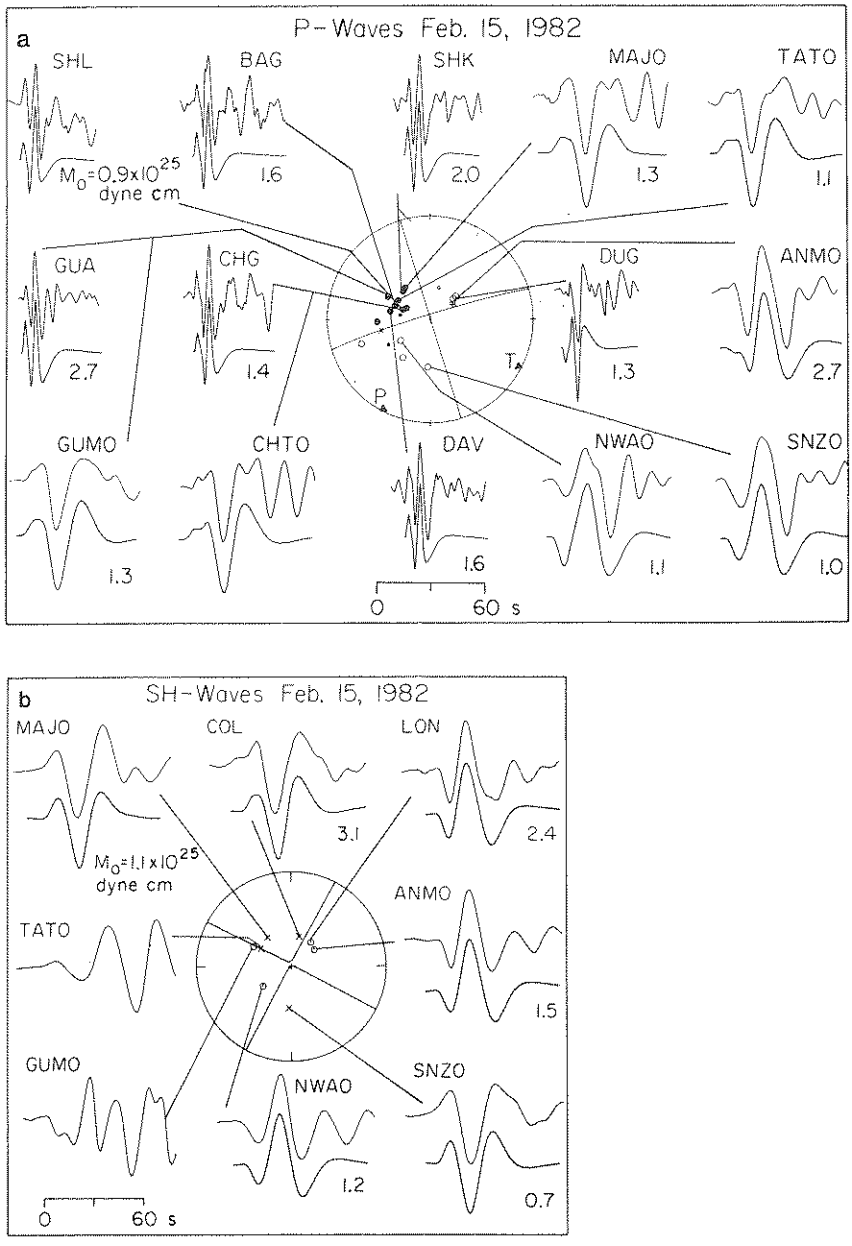

Fig. 6. P wave (a) and SH wave (b) observations and half-space synthetic seismograms for the event of February 15, 1982. The P-wave focal mechanism is shown in a lower hemisphere equal area projection, with solid symbols indicating compressional first arrivals. No moment is given for CHTO because of uncertainty in the gain, and synthetics are not shown for the nodal SH observations. The half-space models have a source depth of 13 km, and all other parameters are as given in Table II.

bars. This indirect determination of source area leads to substantial uncertainty in the stress drops, and we do not place great confidence in the results.

The orientation of the event on February 15 is significantly better constrained. Figure 6 summarizes the body-wave modeling, and it is clear that a nearly pure strike-slip orientation is re-

quired. Note the dramatic increase in the relative amplitude of the second upswing in the WWSSN P waveforms compared to those in Fig. 5. A source depth of 13 km was adopted, with this value being quite well-constrained for the source velocities used. A shorter duration time function with a length of 1.2 s (0.4, 0.4, 0.4) was also required by the high-frequency data. The P waves give an

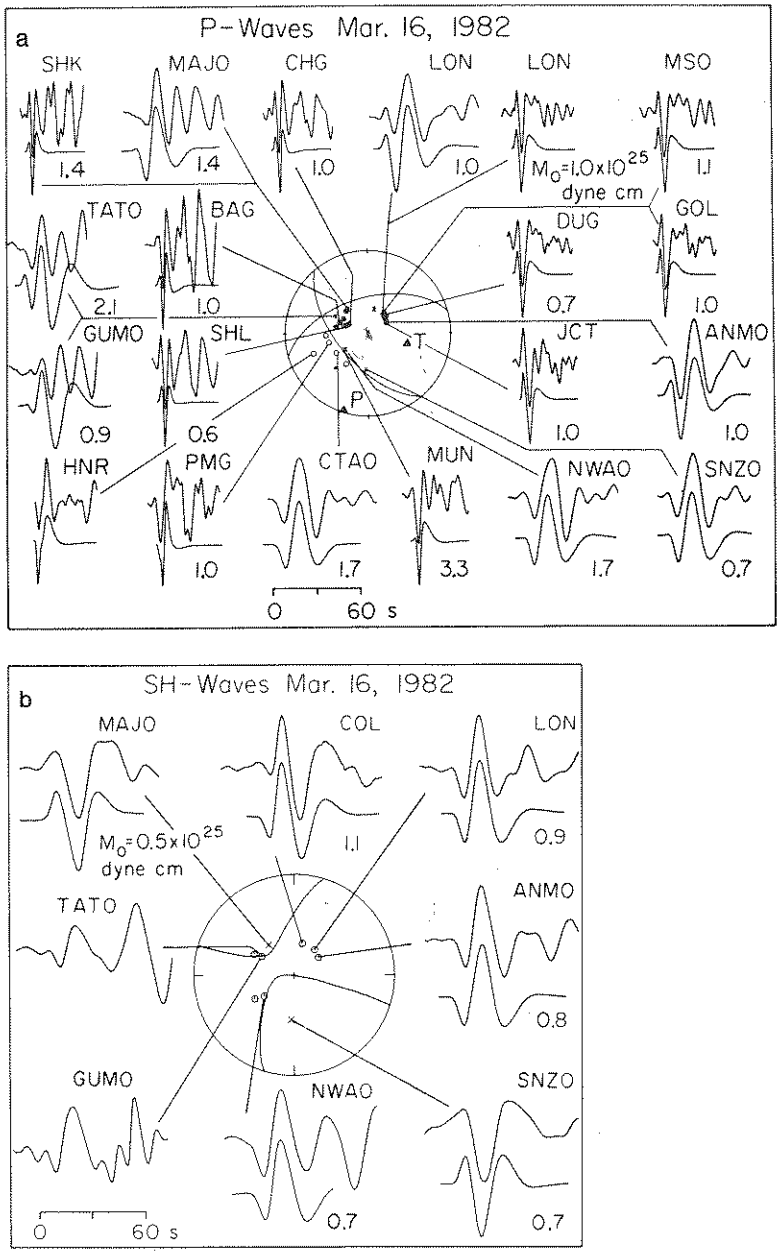

Fig. 7. P wave (a) and SH wave (b) observations and half-space synthetic seismograms for the event of March 16, 1982. The P-wave focal mechanism is shown in a lower hemisphere equal area projection, with solid symbols indicating compressional first arrivals. The moment from each station comparison is given, except for HNR which is at upper mantle distance. Synthetics are not shown for the nodal SH observations. The half-space models have a source depth of 10 km, and all other parameters are as given in Table II.

average moment of 1.5×10^{25} dyne cm and the SH waves yield 1.6×10^{25} dyne cm. The overall average body-wave moment is 1.6×10^{25} dyne cm. The source orientation is $\phi = 253°$, $\delta = 86°$, and $\lambda = 0°$. The fault area is estimated to be 10 km^2, and the stress drop is ~ 1200 bars, with an uncertainty of a factor of at least 2 or 3.

The March 16 event is similar to that of January

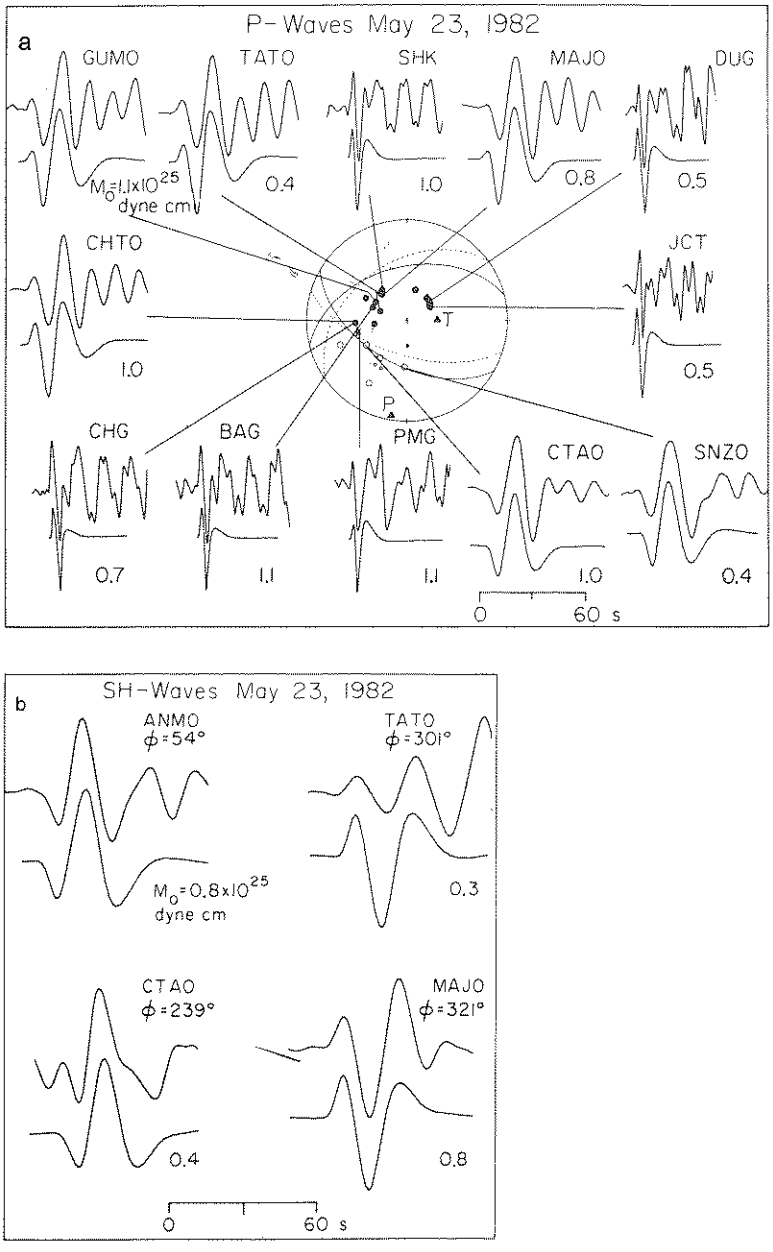

Fig. 8. P wave (a) and SH wave (b) observations and half-space synthetic seismograms for the event of May 23, 1982. The P-wave focal mechanism is shown in a lower hemisphere equal area projection, with solid symbols indicating compressional first arrivals. The half-space models have a source depth of 10 km, and all other parameters are as given in Table II.

7, except that the oblique component is somewhat greater. This is apparent in Fig. 7, which summarizes the P and SH modeling. Note the increase in the second upswing amplitude at BAG, SHK, and CHG and the strong secondary arrivals at stations to the west and northwest. The latter arrivals are P-wave multiples in the water as shown below, and their large relative amplitudes are due to the proximity of the double node for direct P. The upgoing energy at these azimuths ($_{p}P$, $_{p_w}P$) is very strong, producing strong late arrivals. For the half-space models a depth of 10 km and a 2 s duration (0.5, 1.0, 0.5) time function were used. The P waves give an average moment of 1.2×10^{25} dyne cm and the SH waves yield 0.8×10^{25} dyne cm. The combined average is 1.1×10^{25} dyne cm. The source parameters are $\phi = 140°$, $\delta = 60°$, $\lambda = 138°$. The estimated area is 29 km^2, for which the stress drop is 173 bars.

The fourth event modeled, that of May 23, 1982, is similar to the January and March events, as shown in Fig. 8. The amount of oblique slip is closest to that of the January 7 mechanism ($\phi = 120°$, $\delta = 54°$, $\lambda = 120°$), and the waveforms at common stations are very similar. The SH polarity at MAJO is the major feature constraining the oblique contribution. The P waves yield an average moment of 0.8×10^{25} dyne cm and the SH waves give 0.6×10^{25} dyne cm, with the combined average being 0.7×10^{25} dyne cm. The time function has a 1.5 s duration (0.5, 0.5, 0.5), and a 10 km deep source. The m_b of this event is 5.9, the largest of the four events, yet the moment is the smallest. The source area is estimated to be 16–19 km^2, and the stress drop would then be from 213 to 255 bars. The waveforms are not sensitive enough to resolve between the dashed and solid line mechanisms shown in Fig. 8.

Because the depth determinations for these events are of interest, and the half-space modeling is rather crude, we refined the models by incorporating the water layer, which is 5 km thick, and the effects of a crustal layer at the source. The source structure adopted is the same as that used by Stewart and Helmberger (1981) in modeling the 1978 Bermuda Island earthquake. This consists of a 5 km thick crust with a P velocity of 6.3 km s^{-1} overlying a half-space with a P velocity of 8 km s^{-1}. P-wave synthetics were computed using the same 22 ray set shown in Fig. 5 of Stewart and Helmberger (1981) to account for the crustal and water layer reverberations. Using this structure, and the fault orientations determined above, we determined new source depths for each event. The depths found, including the 5 km thick water layer, are $d = 15$ km for January 7, March 16, and May 23, and $d = 21$ km for February 15. Thus, the strike-slip mechanism appears to have a slightly greater depth though the uncertainty is about ± 3 km. The synthetics for several of the WWSSN stations for the layered and half-space models are compared with the data in Fig. 9. Note that there is little difference in the first 15 s of the synthetic waveforms, indicating the adequacy of the half-space modeling for constraining the mechanism. Clearly, accounting for the water and crustal multiples significantly improves the waveform agreement later in the record. In some cases the relative amplitudes of the direct P wave and water multiples are not completely satisfied, but these are generally for nodal direct arrivals, and the uncertainty in take-off angles precludes refining the source. In almost all cases the waveform agreement is quite good for the first 20 s. There is a similar improvement in the fit to the digital network observations when the water multiples are included, particularly 20 s and more into the records, but no additional resolution of the fault mechanisms is obtained.

Fitting the relative timing between the direct arrivals and the water multiples does improve the depth resolution somewhat, as shown in Fig. 10. This figure shows the effect of varying source depth on the synthetic waveforms for two records of the January 7 event. A depth of ~ 15 km is quite consistent with the data for the selected source region model. As was found for the 1978 Bermuda Island earthquake (Stewart and Helmberger, 1981) the events are either subcrustal or located deep in the oceanic crust. The focal mechanisms determined by the body waves are summarized in Table II.

The short-period signals for these events recorded by the GDSN were also inspected in an attempt to constrain the mechanisms and source depths. Representative data are shown in Fig. 11.

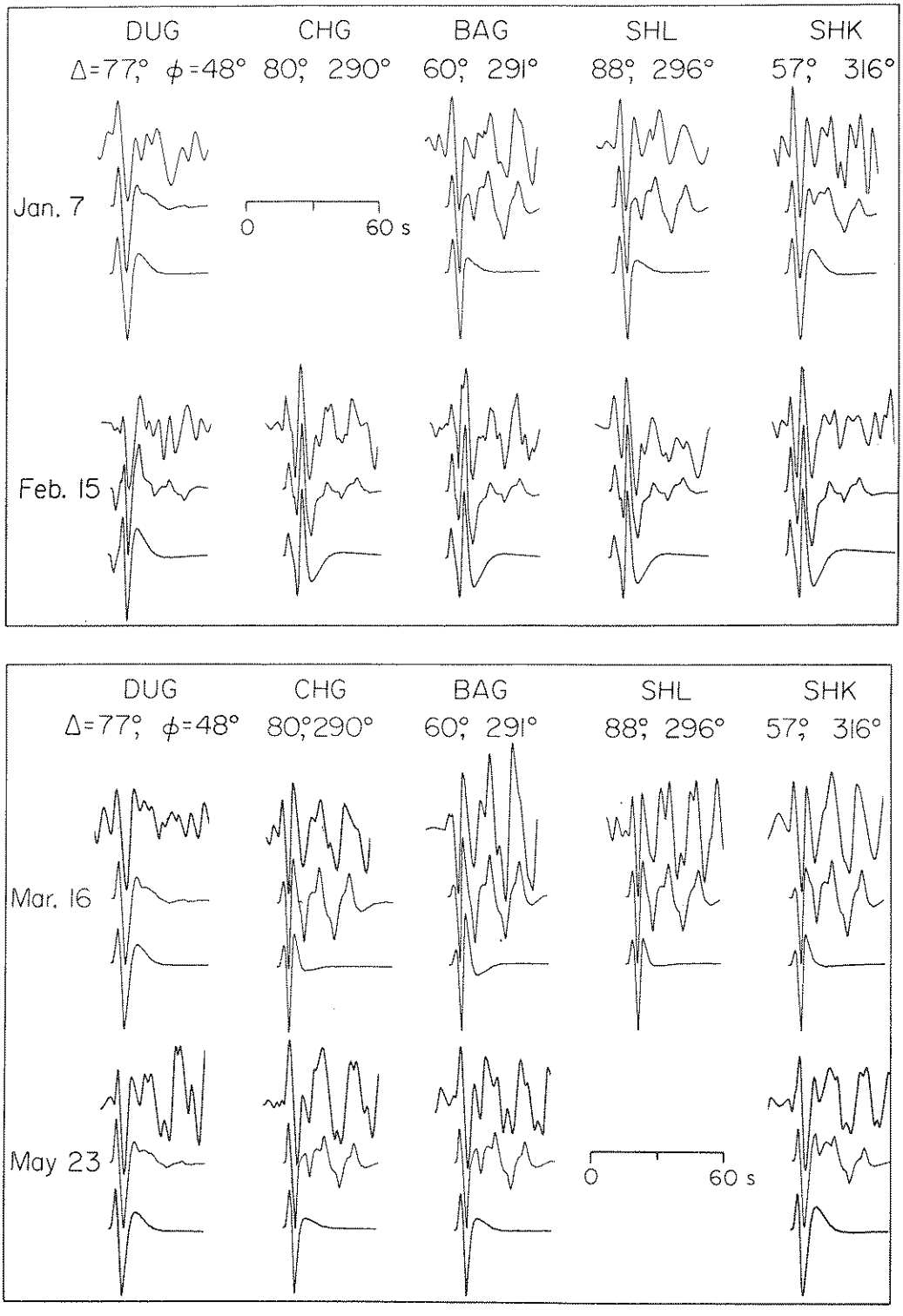

Fig. 9. Comparison of WWSSN observations (top trace), synthetics including reverberations in a layered crust and water layer (middle trace), and half-space synthetics (bottom trace) for the four swarm events. The layered structure calculations provide a more detailed match to the entire waveform, but the first 15 s are well-modeled by the half-space synthetics as well. The mechanisms in Table II are used in the synthetics, except that the half-space models have the source depths given in Figs. 5–8. The strong water-layer multiples for the event of March 16 at azimuths near 290° are produced by the oblique component of slip.

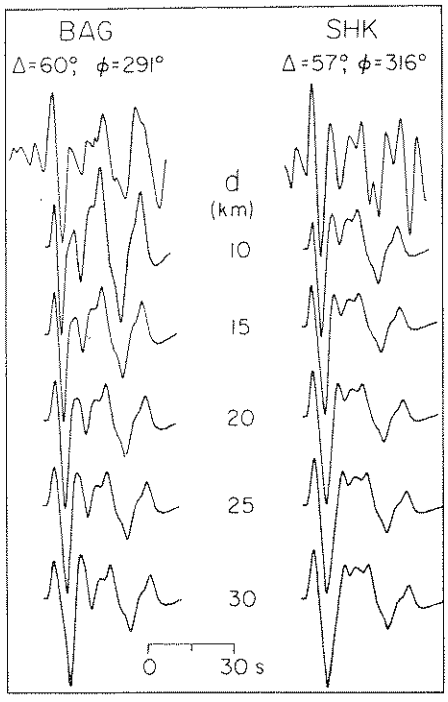

Fig. 10. An illustration of how modeling the time separation between the direct P arrival and the water multiples helps to constrain the source depth. The top row shows observations for the event of January 7, 1982, and the other rows show synthetics for varying source depths in the layered source model.

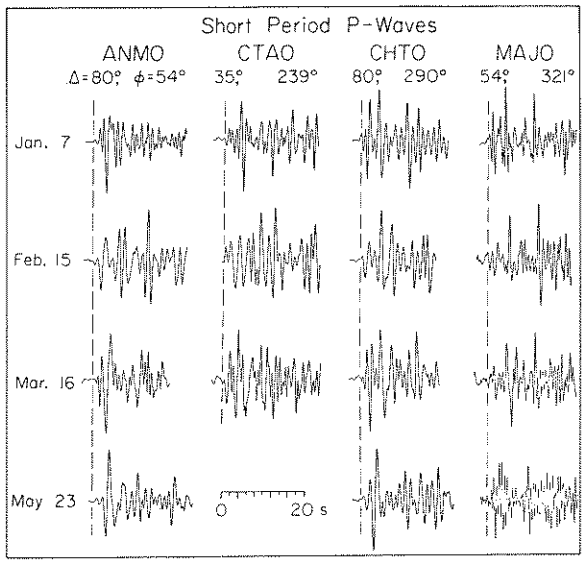

Fig. 11. Comparison of short-period P waves recorded by the GDSN stations. The traces are aligned on the JB arrival time for the NEIS locations. Note the lack of coherence from station to station for a given event and between events. Also note the presence of the small precursory arrivals of variable polarity. These complexities indicate a complicated stress environment.

The traces are aligned on the JB arrival time for the NEIS locations. Several features of these waveforms are of interest. There is very little coherence from event to event at a given station. This variation is more pronounced than apparent in synthetic short-period signals generated using the long-period body-wave models. This suggests a rather complicated failure process. There also appears to be precursors to several of the events that have variable first motions, which are sometimes inconsistent with the visible first motions of the long-period arrivals. This accounts for the many inconsistent polarities reported by stations in the NEIS bulletins for these events. The precursors appear to be source related, though this data cannot rule out possible multipathing effects. These complexities, along with the oblique slip mechanisms, make it difficult to identify surface bounces at all stations. Qualitative comparisons with the synthetics do not indicate different focal depths than the long-period records.

In order to further refine the source models and

TABLE II

Bodywave mechanisms

Event (1982)	h (km)	ϕ,°	δ,°	λ,°	t_1	t_2	t_3	M_o, P [a]	M_o, SH [a]
January 7	15	125	60	120	1.0	1.0	1.0	1.1	0.8
February 15	21	253	86	0	0.4	0.4	0.4	1.5	1.6
March 16	15	140	60	138	0.5	1.0	0.5	1.2	0.8
May 23	15	120	54	120	0.5	0.5	0.5	0.8	0.6

[a] Moment in units of 10^{25} dyne cm.

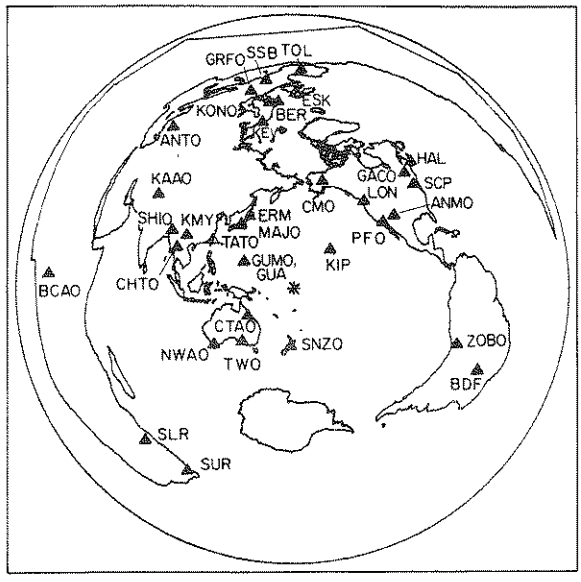

Fig. 12. Equidistance-azimuthal plot centered on the Gilbert Islands swarm source region. The distribution of IDA and GDSN stations used in the surface wave analysis is shown. Not all stations were useable for each event.

to confirm the moment estimates for these four swarm events, the long period Rayleigh- and Love-wave signals recorded at GDSN and IDA stations were analyzed. Figure 12 shows the distribution of digital stations about the source region. At all stations the R_1, R_2, G_1, and G_2 signals were inspected. Those with favorable signal-to-noise ratios at periods > 150 s were processed following the methods described by Kanamori and Given (1982). As discussed in that paper, it is possible to invert the spectral amplitudes of the Rayleigh and Love waves for either moment tensor or fault model solutions. However, because of the shallow depth of the events, a stable inversion for all 5 elements of the moment tensor is not possible. By constraining $M_{xz} = M_{yz} = 0$, one can invert for M_{xy}, M_{yy}, and M_{xx}. In turn, this solution can be decomposed into two double couples with pure strike-slip and 45° dip-slip orientations. This procedure provides good resolution of the strike of the null axis and a first-order estimate of the moment. It also indicates whether the mechanism is predominantly strike-slip or dip-slip, with the relative size of the double couples indicating the proportion of oblique component. Table III lists the results of the constrained moment tensor inversions using source depths of 16 km for each event. Note that the strike-slip orientation is preferred for the February 15 event, and the dip-slip solution is preferred for the other three. The second double couple is small for the events of February 15 and May 23, but increases significantly for the January 7 and March 16 events. These solutions are quite stable for the period range from 150 to 180 s and do not change significantly if only the Rayleigh-wave data is inverted.

Following the procedures described in Kanamori and Given (1982) and Lay et al. (1982) the spectral data were inverted for fault models where the body-wave mechanisms were used as starting models for the non-linear inversions. Several cases were examined, with the least constrained parameters in the body-wave models being allowed to vary. The first case was with the body-wave orientation constrained and the surface-wave spectral data (amplitude and phase) inverted to find the moment. The second case was with the body-wave orientation constrained and the spectral amplitudes alone inverted for the moment. Other models allowed the amount of rake to

TABLE III

Simultaneous Rayleigh and Love wave constrained moment tensor inversion ($M_{zx} = M_{zy} = 0$) $T = 150.59$ s, $d = 16$ km

Event (1982)	M_{xy} [a]	$M_{yy} - M_{xx}$ [a]	$M_{yy} + M_{xx}$ [a]	M_0 [a]	ϕ,°	δ,°	Minor DC, %
January 7	0.420 ± 0.079	0.184 ± 0.165	-0.652 ± 0.118	0.76	128.8	45.0	14.0
February 15	0.741 ± 0.093	1.437 ± 0.201	-0.063 ± 0.120	1.10	248.0	90.0	5.9
March 16	0.450 ± 0.112	0.583 ± 0.237	-0.540 ± 0.145	0.81	118.5	45.0	33.0
May 23	0.159 ± 0.036	0.519 ± 0.084	-0.658 ± 0.051	0.66	105.8	45.0	3.7

[a] Units of moment tensor elements are 10^{25} dyne cm.

vary or the strike to vary. The moment estimates for the first two cases are listed in Table IV. The spectral data are shown in Fig. 13, along with three solutions. The solid lines indicate the predicted spectra for the major double couple of the constrained moment tensor inversions. The dashed lines indicate the results for case 1, described above, and the dotted lines indicate the results for case 2.

For all four events the body-wave solutions are quite compatible with the major double couple of the moment tensor inversion. The poorest agreement is for the event of January 7, for which the body-wave mechanism rotates the lobes of the surface-wave radiation patterns $\sim 30°$ from the moment tensor solution. If we fix the strike and dip of the steeply dipping fault plane in the body-wave mechanism and invert for the rake, the inversion returns a pure dip-slip solution similar to the constrained moment tensor result. If the rake and dip are fixed and the strike is inverted for, the inversion rotates the strike by 28°. Body-wave synthetics for this orientation are not consistent with several of the SH data. In all cases the amplitude inversion gives a moment of 1.0×10^{25} dyne cm. It appears that the exact orientation of this event is simply not well resolved, mainly because the Love-wave data are rather noisy and the body-wave data are sparse. Since the body-wave mechanism appears somewhat more reliable we prefer it for this event, though the uncertainty in ϕ and λ is $\pm 10°$.

The body- and surface-wave solutions are in better agreement for the other three events. For the February 15 event the orientations are nearly identical, though the surface-wave moments (Table IV) are somewhat smaller than the body-wave moments. In this case the surface-wave moment may be more reliable due to the large number of nodal body waves. The March 16 event is a somewhat better fit by the body-wave solution because the oblique slip enhances the relative excitation of the Love waves. For this event the minor double couple of the moment tensor inversion is large, and the fit to the spectral data is correspondingly poor for the major double couple alone. The moment for the amplitude inversion is 1.2×10^{25} dyne cm compared with 1.1×10^{25} dyne cm obtained from the body waves. As with the event of January 7, if the rake is allowed to vary as well, a more dip-slip dominated mechanism is returned ($\lambda = 120°$ compared to $\lambda = 138°$ for the body-wave solution). Inverting for the strike gives a solution that is rotated by 17°, which moves the Rayleigh-wave maxima onto the cluster of large Rayleigh-wave amplitudes. Either model produces a slightly poorer fit to the body-wave data, and again we feel that the body-wave orientation is the best model given the intrinsic uncertainty in the modeling. The spectral data are somewhat suspect because of the observed scatter in the phase which indicates that for the period (150.59 s) and particular paths involved the great circle average phase velocities used in the inversion are inappropriate. The May 23 event shows good agreement between the surface-wave data and the body-wave models, in both orientation and moment.

The body-wave constrained mechanisms are compared with the orientation of the major double couple of the constrained moment tensor inversions in Fig. 14. The moments shown are the preferred values determined by averaging the body-wave results and the surface-wave amplitude inversion determinations. Note that the principal features of the mechanisms are resolved by the moment tensor inversions, and the most consistent aspect from event to event is the horizontal orientation of the compression axis trending NNE–SSW. These mechanisms are quite similiar to those determined by moment tensor inversions of the body-wave trains observed at GDSN stations performed at Harvard, which are tabulated by the NEIS.

TABLE IV

Moments for surface-wave fault inversions using body-wave constrained orientations

Event (1982)	ϕ,°	δ,°	λ,°	M_0 [a]	M_0 [b]
January 7	125	60	120	0.69	0.96
February 15	253	86	0	1.01	1.19
March 16	140	60	138	0.81	1.16
May 23	120	54	120	0.68	0.76

[a] Moment using amplitude and phase spectra, in units of 10^{25} dyne cm.

[a] Moment using amplitudes only, in units of 10^{25} dyne cm.

3. Discussion

The four earthquakes analyzed in detail above appear to be representative of the range of mechanisms associated with the Gilbert Islands swarm. Several smaller events in 1982 have been analyzed by Harvard, and their mechanisms are reported by the NEIS, but their moments are too small for the

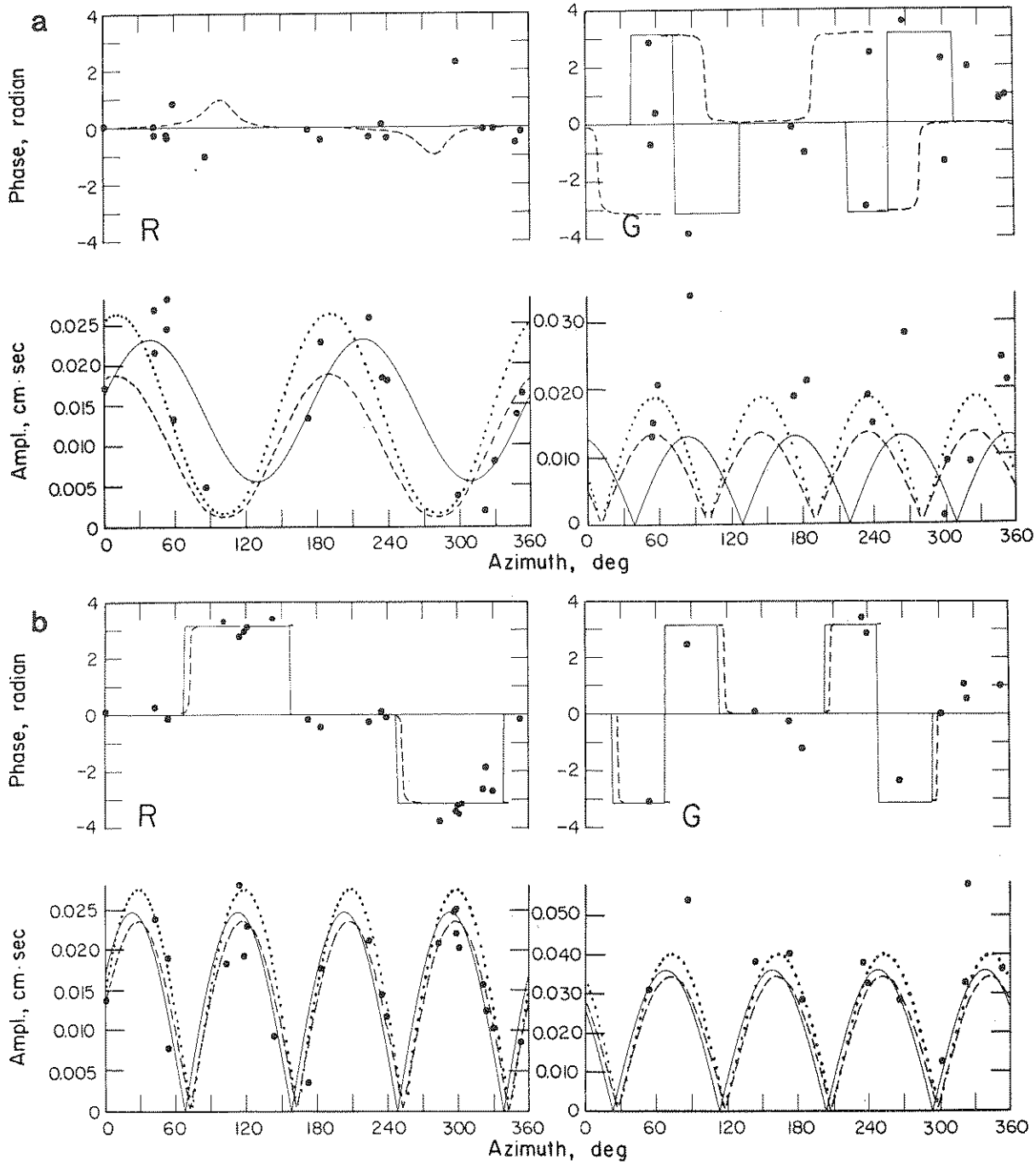

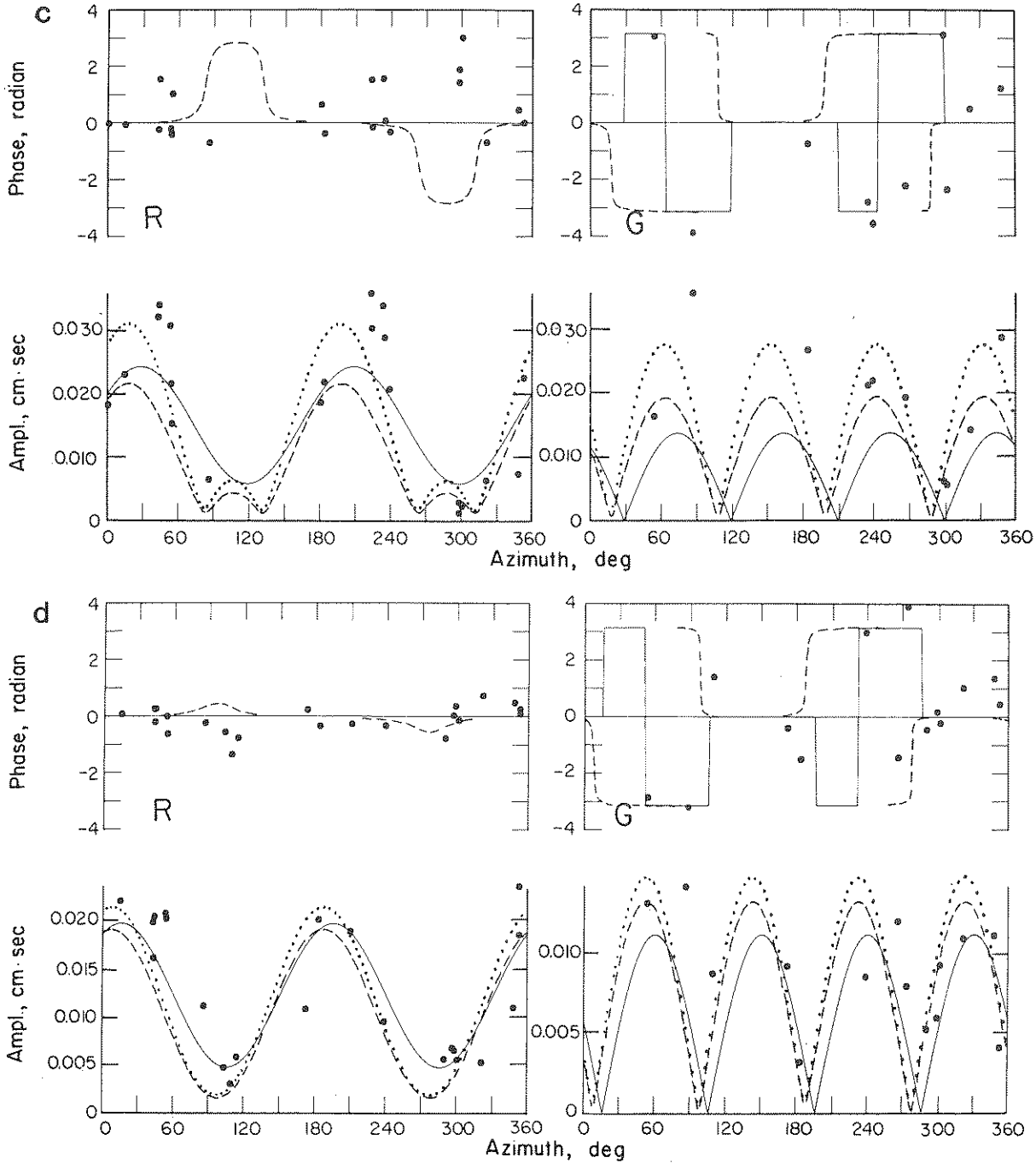

Fig. 13. Rayleigh-wave (R) and Love-wave (G) amplitude and phase spectra for 150.59 s period observations and inversion models. The events are (a) January 7, 1982, (b) February 15, 1982, (c) March 16, 1982, and (d) May 23, 1982. For each event three solutions are shown. The solid line is the result for the major double couple of the constrained moment tensor inversion tabulated in Table III. The dashed line is the result of a fault model inversion for moment using both amplitude and phase information with the orientation constrained to be that determined by the body waves (Table II). The dotted line is for a similar inversion using only the amplitude spectra. The moments for the latter two cases are listed in Table IV.

procedure we employ in this paper. In all cases, the common feature of the mechanisms is the consistent NNE-SSW horizontal orientation of the compression axis. Thrusting-type mechanisms appear to dominate in the sequence, though the oblique component varies from event to event.

Though the variability of the focal mechanisms presents some problems, the total moment release of the swarm can be estimated at $\sim 1.0 \times 10^{26}$ dyne cm, or about the moment release for a magnitude 7 earthquake. This value can be compared to the total moment release equivalent to a $M = 6.3$ earthquake ($\sim 2.0 \times 10^{25}$ dyne cm) estimated for the 1965–1968 Matsushiro swarm (Hagiwara and Iwata, 1968), and the lower boundary of 1.5×10^{26} dyne cm for the total moment released in the swarm accompanying the Fernandina caldera collapse (Kaufman and Burdick, 1980). Okal (1983) has estimated that the annual moment release from all of the globally distributed intraplate earthquakes since 1964 listed by Bergman and Solomon (1980) is slightly less than 1.0×10^{26} dyne cm y^{-1}. This, along with the fact that the only other magnitude 6 or greater intraplate seismic activity recorded in the entire Pacific plate, with the exception of the Hawaiian hot spot, is concentrated in the extreme southern tip of the plate or in the vicinity of the East Pacific Rise (Okal, 1983), indicates the unusually large size of the Gilbert Islands swarm.

The Gilbert Islands swarm does not have a clear precedent, and it is of interest to consider the origin of the stress release and the location of the seismicity. The occurrence of an intraplate swarm of large magnitude thrusting events runs contrary to previous observations and models of swarm activity. Most swarms occur in regions of thin, heterogeneous crust in rifting environments, which are often associated with magmatic activity. Typical oceanic swarms are normal or strike-slip faulting events near ridge or transform segments of the Mid-Oceanic Ridge system (Sykes, 1970; Tatham and Savino, 1974). Intraplate swarms have been documented in connection with volcanism, either prior to or during episodes of eruption [e.g., at Mauna Loa, Koyanagi et al. (1975); and near Tahiti, Talandier and Okal (1983)], or associated with post-eruptional caldera collapse such as at Fernandina, Galapagos Islands in 1968 (Filson et al., 1973; Kaufman and Burdick, 1980). However, these events involved normal faulting, and the former have been of a much lower magnitude, while the latter have had much shorter duration, than the Gilbert Islands swarm. Stein (1978) has studied the Chagos–Laccadive swarm of 1965–1970 in the Indian Ocean, also characterized by normal faulting, and concluded that it may have resulted from failure along a fossil fracture in the lithospheric plate, in the immediate vicinity of a major bathymetric feature. Only 16 events were detected in that 'swarm', with the largest event having a moment of 6.8×10^{25} dyne cm, almost an order of magnitude larger than the next largest events.

There is no record of a previous large magnitude swarm with predominantly thrust faulting in any ocean basin. In fact, very few swarms anywhere are known to have thrust-faulting mechanisms. Examples are the Santa Barbara swarm of 1968 (Sylvester et al., 1970), which is believed to have had oblique thrusting, and the Blue Moun-

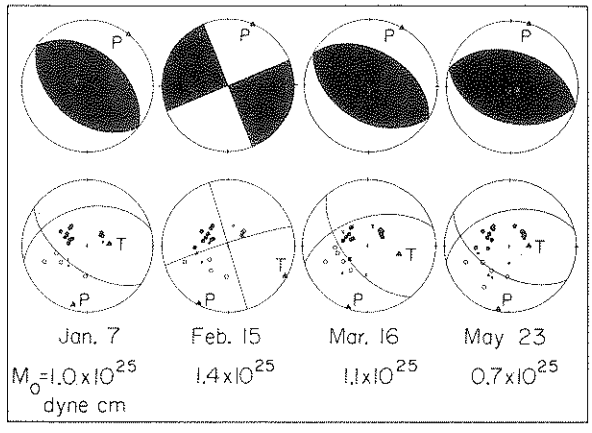

Fig. 14. Summary of the focal mechanisms and moment determinations for the four largest events of the Gilbert Islands swarm. The top row shows the orientation of the major double couple found by the constrained moment tensor inversions of the surface waves. The shaded quadrants are compressional first motion. The bottom row shows the body-wave constrained mechanisms along with P-wave first motion data. Note the consistent orientation of the compressional (P) axes despite the variation in orientation. The moments are the preferred values obtained by averaging the body-wave and surface-wave amplitude fault inversion results.

tain Lake swarm in 1971–1972 (Sbar et al., 1972). These were both small magnitude swarms. It is important to note that most intraplate oceanic events well-removed from volcanic centers occur as single, isolated earthquakes, with very few aftershocks being detected. Thus, the occurrence of a swarm in the Gilbert Islands is in itself an unusual event.

The Gilbert Islands swarm is also unusual because of its principal stress orientation. Typical oceanic earthquakes, especially in areas more than a few million years old, have predominantly horizontal compression axes, that are often oriented in the direction of ridge spreading (Mendiguren, 1971; Sykes and Sbar, 1974; Okal, 1980), which has been interpreted as resulting from the ridge-push system of gravitational sliding forces (e.g., Mendiguren and Richter, 1978; Okal, 1983; Wiens and Stein, 1983). Occasionally, major fossil bathymetric features appear to distort or even control the orientation of the stress release (Raleigh et al., 1972; Stein, 1979; Bergman and Solomon, 1980). In the present case, the orientation of the compressive stress is clearly not parallel to the direction of plate motion; rather it is orthogonal to it, and the tension axis is variable and generally not aligned with the plate motion either. In this respect, the Gilbert Islands swarm differs fundamentally from the seismicity observed at Regions 'A' and 'C' in the south-central Pacific by Okal et al. (1980), for which the mechanisms are consistent with a ridge-push force system. The latter events also had lower b-values. The stress drops and fault areas estimated from the body waves are comparable to those found for isolated intraplate oceanic events (Liu and Kanamori, 1980), which tend to be in the order of several hundred bars.

The Gilbert Islands are probably old features and there is no evidence of a major bathymetric feature near the epicenter. Thus, there would be no a priori reason to expect either magmatic activity or a locally induced preferred stress orientation in the region. On the other hand, the events did occur at the southeastern end of the Gilbert Island chain, where any new island formation might be expected to occur if a recent hot spot had produced the islands. The offset in the island chain between the Gilbert and Ellice Islands is not defined by any clear bathymetric feature, such as a fracture zone, which would serve as a zone of weakness, though this does not preclude the existence of such a weak region within the lithosphere. The focal mechanisms in Fig. 14 have one fault plane that is fairly consistent from event to event, that trending WSW. This azimuth roughly corresponds to the direction along which the Island chain is offset. Since this plane is the least well-constrained and varies in dip, it is not clear whether this is a fortuitous result.

The exact origin of the Gilbert Islands is rather obscure. Magnetic anomaly data (Larson and Chase, 1972) suggest that this portion of the ocean floor was generated ~ 115 Ma ago, at the now defunct Phoenix–Pacific ridge. The magnetic anomalies in the sea-floor eastward of the swarm epicenter increase in age in a northerly direction, parallel to the trend of the Marshall–Gilbert Island Chain. An offset of ~ 8 Ma in the anomalies delineates a probable NNW–SSE trending fracture zone in the original ridge system, roughly aligned with the epicentral region. Larson and Chase (1972) propose that this feature is an extension of the Louisville Ridge–Eltanin fracture zone lineation. Such fossil features have been recognized as zones of weakness along which intraplate oceanic seismicity occurs (e.g., Okal, 1983). Even fracture zones in very old oceanic lithosphere have the potential to influence stress release, as for the Bermuda earthquake of 1978 (Stewart and Helmberger, 1981). The Gilbert Islands themselves are presently all coral reefs. The signature in the geoid of the Gilbert Islands is quite sharp (Parke et al., 1982), indicating that they are uncompensated and were generated off-ridge. The geoid signature of the Ellice Islands, on the other hand, is very weak, and thus they were probably generated at or near the ridge crest. If the same mantle source produced the two island systems, the ridge must have caught up with them, possibly by an episode of ridge jumping, a process also known to result in weakness of the lithospheric plate. However, this would have taken place during the Cretaceous, during a period of magnetic reversal quiescence, and would hence be undocumented in the magnetic record. Furthermore, Henderson and Gordon (1981; personal communication, 1983) have sug-

gested that the Gilbert Islands may have been generated by the Society Islands (Tahiti) hot spot, while the Ellice Islands have a different source. No ridge jump would then be necessary to explain the difference in compensation of the two island groups. It is clear that our present knowledge of the bathymetry and tectonic history of the region is insufficient to account of the occurrence of the seismicity in the Gilbert Islands region.

The possibility that there is a volcanic origin for the swarm must also be considered. Given the absence of other evidence for present-day volcanism in the area, and the apparently large age of the seamounts in the region, such an explanation is rather speculative. Any ongoing volcanism in the region would have left no trace of its activity for the past 5 Ma or so (about the length of time required to reduce a hot spot-type island to atoll status), and the sudden onset of activity would be hard to account for. An examination of individual SEASAT tracks in the epicentral region failed to identify any uncharted seamounts comparable, say, to the MacDonald Volcano. The moderately high b-value of 1.35 is comparable to that of the 'A' type earthquakes in Minakami's classification (Minakami, 1974; McNutt, 1983), and the long duration and sustained high peak magnitudes of the swarm activity do suggest a steady driving stress such as might accompany repeated magma injections. The larger earthquakes occurred rather deep in the crust, and no surface expression of the activity is necessarily expected. The Gilbert Islands swarm does differ from swarms in documented volcanic areas in that such swarms are usually much shorter-lived, with a few weeks duration (Sykes, 1970; Francis, 1974; Endo et al., 1981), and they rarely, if ever, feature a trend of horizontal compressional axes. The variability of the focal mechanisms and the complexity of the short-period signals indicate a complex stress environment, and it is quite possible that a combination of a pre-existing zone of weakness and some magmatic activity could account for the swarm.

It is interesting to note that the area north of the Samoa Islands (from 6° to 10°S, and 173° to 179°W) had repeated seismicity in 1956, 1957 and 1964, with another possible event in 1940 (Greenberg and Okal, 1983). While these events cannot be analyzed in detail, it does appear that large scale sustained deformation of the Pacific plate is occurring in this region. Very long-baseline geodetic measurements between the numerous islands in this part of the Pacific plate may shed light on the nature of intraplate deformation within oceanic plates.

4. Conclusions

The earthquake swarm which occurred in the Gilbert Islands between December 1981 and March 1983 is one of the most unusual intraplate events recorded. No prior seismic or volcanic activity has been reported in the source region in the historical record. The swarm produced 217 earthquakes that were located by the NEIS, with the largest magnitudes being $m_b = 5.8$–5.9. Most of the earthquake mechanisms determined by body- and surface-wave analysis have predominantly thrust orientations with substantial oblique components, while some events are pure strike-slip. The mechanisms have consistent compression axes, oriented horizontally and trending NNE–SSW. The stress orientation is orthogonal to the direction of plate motion, and there is no bathymetric feature clearly associated with the fault orientations. The swarm occurred near an offset of the Gilbert and Ellice Island groups, which may be a zone of weakness, though the cause of the offset is not understood. It is not possible to resolve whether a magmatic event or regional tectonic stresses are responsible for the swarm activity at this time.

Acknowledgments

We thank Hiroo Kanamori and Terry Wallace for discussions about this sequence, and Anny Cazenave for accessing and interpreting the SEASAT data. Cindy Arvesen typed the manuscript. This research was supported by the National Science Foundation under Grants EAR 81-15236 (Caltech) and EAR 81-06106 (Yale), and the Office of Naval Research under Contract N00014-79-C-0292. Contribution number 3914, Division of Geological and Planetary Sciences,

California Institute of Technology, Pasadena, CA 91125.

References

Aki, K., 1965. Maximum likelihood estimate of b in the formula log N = a – bM and its confidence limits. Bull. Earthquake Res. Inst. Tokyo Univ., 43: 237–239.

Bergman, E.A. and Solomon, S.C., 1980. Oceanic intraplate earthquakes: Implications for local and regional intraplate stress. J. Geophys. Res., 85: 5389–5410.

Ebel, J.E., Burdick, L.J. and Stewart, G.S., 1978. The source mechanism of the August 7, 1966 El Golfo earthquake. Bull. Seismol. Soc. Am., 68: 1281–1292.

Endo, E.T., Malone, S.D., Noson, L.L. and Weaver, C.S., 1981. Location, magnitudes and statistics of the March 10–May 18 earthquake sequence. U.S. Geol. Surv. Prof. Pap., 1250: 93–107.

Filson, J., Simkin, T. and Leu, L., 1973. Seismicity of a caldera collapse: Galapagos Islands 1968. J. Geophys. Res., 78: 8591–8622.

Francis, T.J.G., 1968. The detailed seismicity of mid-ocean ridges. Earth Planet. Sci. Lett., 4: 39–46.

Francis, T.J.G., 1974. A new interpretation of the 1968 Fernandina caldera collapse and its implications for the mid-ocean ridges. Geophys. J.R. Astron. Soc., 39: 301–318.

Furumoto, A.S., Nielsen, N.N. and Phillips, W.R., 1973. A study of past earthquakes, isoseismic zones of intensity, and recommended zones for structural design for Hawaii. Report HIG-73-4, Hawaii Inst. Geophys., 100 pp.

Greenberg, J.G. and Okal, E.A., 1983. Intraplate seismicity of the southern part of the Pacific plate, EOS, Trans. Am. Geophys. Union, 64: 269.

Groves, G.W., 1983. Earthquakes at Arorae Island, Kiribati, 1982. Institute of Marine Resources Atoll Research Unit Technical Report, Bikenibeu, Tarawa, Republic of Kiribati., 21 pp.

Gutenberg, B. and Richter, C.F., 1954. Seismicity of the Earth and Associated Phenomena. 2nd edn., Princeton University Press, Princeton, NJ, 310 pp.

Hagiwara, T. and Iwata, T., 1968. Summary of the seismographic observations of Matsushiro swarm earthquakes. Bull. Earthquake Res. Inst. Tokyo Univ., 46: 485–515.

Henderson, L.J. and Gordon, R.G., 1981. Oceanic plateaus and the motion of the Pacific plate with respect to hot spots. EOS, Trans. Am. Geophys. Union, 62: 1028.

Langston, C.A. and Helmberger, D.V., 1975. A procedure for modeling shallow dislocation sources. Geophys. J. R. Astron. Soc., 42: 117–130.

Kanamori, H. and Given, J.W., 1981. Use of long-period surface waves for rapid determination of earthquake source parameters. Phys. Earth Planet. Inter., 27: 8–31.

Kanamori, H. and Stewart, G.S., 1976. Mode of the strain release along the Gibbs fracture zone, Mid-Atlantic ridge. Phys. Earth Planet. Inter., 11: 312–332.

Kaufman, K. and Burdick, L.J., 1980. The reproducing earthquakes of the Galapagos Islands. Bull. Seismol. Soc. Am., 70: 1759–1770.

Koyanagi, R.Y., Endo, E.T. and Ebisu, J.S., 1975. Reawakening of Mauna Loa Volcano, Hawaii; a preliminary evaluation of seismic evidence. Geophys. Res. Lett., 2: 405–409.

Larson, R.L. and Chase, C.G., 1972. Late Mesozoic evolution of the western Pacific Ocean. Geol. Soc. Am. Bull., 83: 3627–3644.

Lay, T., Given, J.W. and Kanamori, H., 1982. Long-period mechanism of the 8 November 1980 Eureka, California, earthquake. Bull. Seismol. Soc. Am., 72: 439–456.

Liu, H.-L. and Kanamori, H., 1980. Determination of source parameters of mid-plate earthquakes from the waveforms of body waves. Bull. Seismol. Soc. Am., 70: 1989–2004.

Mammerickx, J., Chase, T.E., Smith, S.M. and Taylor, I.L., 1974. Bathymetry of the South Pacific (map). IMR Tech. Rep. Ser. 45A, Scripps Inst. Oceanogr., Univ. Calif., San Diego, CA.

Matumoto, T. and Ward, P.L., 1967. Microearthquake study of Mount Katmai and vicinity, Alaska. J. Geophys. Res., 72: 2557–2568.

McNutt, S.R., 1983. A review of volcano seismicity. EOS, Trans. Am. Geophys. Union, 64: 265.

Mendiguren, J.A., 1971. Focal mechanism of a shock in the middle of the Nazca plate. J. Geophys. Res., 76: 3861–3879.

Mendiguren, J.A. and Richter, F.M., 1978. On the origin of compressional intraplate stresses in South America. Phys. Earth Planet. Inter., 16: 318–326.

Minakami, T., 1974. Seismology of Volcanoes in Japan. In: L. Civetta, P. Gasparini, G. Luongo and A. Rapolla (Editors), Physical Volcanology. Elsevier, Amsterdam, pp. 1–27.

Okal, E.A., 1980. The Bellingshausen Sea earthquake of February 5, 1977: evidence for ridge-generated compression in the Antarctic plate. Earth Planet. Sci. Lett., 46: 306–310.

Okal, E.A., 1983. Oceanic intraplate seismicity. Annu. Rev. Earth Planet. Sci., 11: 195–214.

Okal, E.A., Talandier, J., Sverdrup, K.A. and Jordan, T.H., 1980. Seismicity and tectonic stress in the south-central Pacific. J. Geophys. Res., 85: 6479–6495.

Parke, M.E., Stavert, L.R. and Hussey, K.J., 1982. Topographic relief from SEASAT altimeter mean sea surface (map). Jet Propulsion Laboratory, Pasadena, CA.

Raleigh, C.B., Healy, H.J. and Bredehoeft, D.J., 1972. Faulting and crustal stress at Rangely, Colorado. In: H.C. Heard (Editor), Flow and Fracture of Rocks. Geophys. Monogr. Ser., 16: 275–284.

Ritsema, A.R., 1958. (i, Δ)-curves for bodily seismic waves at any focal depth. Lembaga Meterologi dan Geofisik, Republik Indonesia, Verhandelingen No. 54.

Sakuma, S. and Nagata, R., 1957. Physical volcanology. Handb. Phys., 48: 982–1011.

Sbar, M.L., Armbruster, J. and Aggarwal, Y.P., 1972. The Adirondack, New York, earthquake swarm of 1971 and tectonic implications. Bull. Seismol. Soc. Am., 62: 1303–1317.

Stein, S., 1978. An earthquake swarm on the Chagos-Laccadive

Ridge and its tectonic implications. Geophys. J. R. Astron. Soc., 55: 577–588.

Stein, S., 1979. Intraplate seismicity on bathymetric features: the 1968 Emperor Trough earthquake. J. Geophys. Res., 84: 4763–4768.

Stewart, G.S. and Helmberger, D.V., 1981. The Bermuda earthquake of March 24, 1978: a significant oceanic intraplate event. J. Geophys. Res., 86: 7027–7036.

Sykes, L.R., 1970. Earthquake swarms and sea-floor spreading. J. Geophys. Res., 75: 6598–6611.

Sykes, L.R. and Sbar, M.L., 1974. Focal mechanism solutions of intraplate earthquakes and stresses in the lithosphere. In: L. Kristjansson (Editor), Geodynamics of Iceland and the North Atlantic Area. Reidel, Dordrecht, pp. 207–224.

Sylvester, A.G., Smith, S.W. and Scholz, C.H., 1970. Earthquake swarm in the Santa Barbara channel, California, 1968. Bull. Seismol. Soc. Am., 60: 1047–1060.

Talandier, J. and Kuster, G.T., 1976. Seismicity and submarine volcanic activity in French Polynesia. J. Geophys. Res., 81: 936–948.

Talandier, J. and Okal, E.A., 1983. The volcano-seismic swarms of 1981 and 1982 in the Tahiti–Mehetia area, French Polynesia. J. Geophys. Res., submitted.

Tatham, R.H. and Savino, J.M., 1974. Faulting mechanisms for two oceanic earthquake swarms. J. Geophys. Res., 79: 2643–2652.

Utsu, T., 1966. A statistical significance test of the difference in b-value between two earthquake groups. J. Phys. Earth, 14: 37–40.

Wiens, D.A. and Stein, S., 1983. Age dependence of oceanic intraplate seismicity and implications for lithospheric evolution. J. Geophys. Res., 88: 6455–6468.